

LA-UR-12-24386

Approved for public release; distribution is unlimited.

Title:	Implementation and Validation of the BHR Turbulence Model in the FLAG Hydrocode
Author(s):	Denissen, Nicholas A. Fung, Jimmy Reisner, Jon M. Andrews, Malcolm J.
Intended for:	Report



Disclaimer:

Los Alamos National Laboratory, an affirmative action/equal opportunity employer, is operated by the Los Alamos National Security, LLC for the National Nuclear Security Administration of the U.S. Department of Energy under contract DE-AC52-06NA25396. By approving this article, the publisher recognizes that the U.S. Government retains nonexclusive, royalty-free license to publish or reproduce the published form of this contribution, or to allow others to do so, for U.S. Government purposes. Los Alamos National Laboratory requests that the publisher identify this article as work performed under the auspices of the U.S. Department of Energy. Los Alamos National Laboratory strongly supports academic freedom and a researcher's right to publish; as an institution, however, the Laboratory does not endorse the viewpoint of a publication or guarantee its technical correctness.

Implementation and Validation of the BHR Turbulence Model in the FLAG Hydrocode

Nicholas A. Denissen, Jimmy Fung, Jon M. Reisner, Malcolm J. Andrews

*Los Alamos National Laboratory**

(Dated: August 28, 2012)

The BHR-2 turbulence model, developed at Los Alamos National Laboratory for variable density and compressible flows, is implemented in an Arbitrary Lagrangian–Eulerian hydrocode, FLAG. The BHR-2 formulation is discussed, with emphasis on its connection to multi-component flow formulations that underlie FLAG’s treatment of multi-species flow. One-dimensional and two-dimensional validation tests are performed and compared to experiment and Eulerian simulations.

I. INTRODUCTION

Turbulence is an often studied and ubiquitous phenomenon in nature, and modeling its effects is essential in many practical applications. Specifically the behavior of turbulence in the presence of strong density gradients and compressibility is of fundamental importance in applications ranging from Inertial Confinement Fusion (ICF)[1], supernovae[2], and atmospheric flows. The BHR closure approach[3] seeks to model the physical processes at work in variable density turbulence including Kelvin-Helmholtz (KH)[4], Rayleigh-Taylor (RT) [5], and Richtmyer-Meshkov (RM)[6], driven turbulence.

The effectiveness of the BHR-2 implementation has been demonstrated for variable density mixing in the KH, RT, and RM cases in an Eulerian framework[7]. The primary motivation of the present work is to implement the BHR-2 turbulence model in the Arbitrary Lagrangian-Eulerian (ALE) hydrodynamics code FLAG. The goal is not only to demonstrate results in agreement with previous Eulerian calculations, but also document behavior that arises from the underlying differences in code philosophy.

*Electronic address: `denissen@lanl.gov`

II. IMPLEMENTATION

FLAG is a multi-dimensional (1,2,3D), multi-physics code, that solves the bulk hydrodynamic equations in a Lagrangian reference frame on an arbitrary polyhedral mesh[8, 9].

$$\frac{D\rho}{Dt} = -\rho \frac{\partial u_j}{\partial x_j} \quad (1)$$

$$\rho \frac{Du_i}{Dt} = -\frac{\partial p}{\partial x_i} + \rho g_i \quad (2)$$

$$\rho \frac{De}{Dt} = -p \frac{\partial u_j}{\partial x_j} \quad (3)$$

FLAG uses a single bulk velocity, but separate mass and energy equations are solved for each species[10]. This results in conservation equations for species concentration, c_i , and specific internal energy, e_i .

The equations are discretized using a compatible, staggered-grid formulation[11], and, when called for, the code follows the Lagrangian hydrodynamics step with a mesh relaxation/remap step[12]. Time integration for the hydrodynamics is a nominally second-order, predictor-corrector scheme. The initial framework for incorporating the effects of turbulence was implemented by Waltz and Gianakon[10]. This work describes the implementation and validation of BHR within that framework.

A. BHR Governing Equations

The derivation of the governing equations and closure assumptions in the BHR framework can be found in Ref. [3], and several “flavors” of BHR can be found as well[7, 13, 14]. Thus a detailed derivation will not be presented here. Rather, the relevant terms, governing equations and their model constants are given and derivations are presented where necessary to highlight characteristics specific to FLAG.

The bulk hydrodynamic equations are now the ensemble averaged Euler equations:

$$\frac{D\bar{\rho}}{Dt} = -\bar{\rho} \frac{\partial \tilde{u}_j}{\partial x_j} \quad (4)$$

$$\bar{\rho} \frac{D\tilde{u}_i}{Dt} = -\frac{\partial}{\partial x_j} (\bar{p} \delta_{ij} + \overline{\rho u_i'' u_j''}) + \bar{\rho} g_i \quad (5)$$

$$\bar{\rho} \frac{D\tilde{e}}{Dt} = -\bar{p} \frac{\partial \tilde{u}_j}{\partial x_j} - \frac{\partial}{\partial x_j} (\overline{\rho e'' u_j''}) \quad (6)$$

where overbars denote standard (ie. volume-weighted) averages and tildes denote mass-weighted averages. Fluctuating quantities are defined as the differences:

$$\phi = \bar{\phi} + \phi' = \tilde{\phi} + \phi''$$

with:

$$\tilde{\phi} = \frac{\overline{\rho\phi}}{\bar{\rho}}$$

Supplementing the bulk equations are transport equations for the species mass fraction:

$$\bar{\rho} \frac{D\tilde{c}_k}{Dt} = - \frac{\partial}{\partial x_j} (\overline{\rho c_k'' u_j''}) \quad (7)$$

and the necessary equations of state.

The goal of the turbulence model is to specify the Reynolds stress tensor:

$$R_{ij} = \overline{\rho u_i'' u_j''}$$

the turbulent energy flux:

$$S_j = \overline{\rho e'' u_j''}$$

the turbulent mass flux:

$$\rho c_k u_{dk,j} = \overline{\rho c_k'' u_j''}$$

and a relationship between the ensemble average and the mass-weighted average:

$$\tilde{u}_i = \bar{u}_i + a_i$$

which by definition:

$$a_i = \frac{\overline{\rho' u_i'}}{\bar{\rho}} = -\overline{u_i''}$$

The BHR family of models derives transport equations for the primary quantities of interest, and uses gradient diffusion approximations for remaining terms and higher-order moments. BHR-2 employs transport equation for the turbulent kinetic energy, $K = R_{ii}/2\bar{\rho}$, the turbulent length scale, L , the mass-flux velocity a_i , and the density self correlation, $b = -\overline{\rho'(1/\rho)'}$. A turbulent viscosity, $\mu_T = \bar{\rho} C_\mu L \sqrt{K}$, and dissipation $\epsilon = K^{3/2}/L$ are formed from these terms. Gradient diffusion approximations are used to close these equations as well as define the turbulent mass flux, $u_{di,j}$, and energy flux S_j . An algebraic closure is used to relate the Reynolds stress to K and L . Note that Ref. [7] uses S for the length scale.

The present implementation strives to maintain consistency with the simpler k - L model also found in FLAG[15].

In Lagrangian form, the turbulence model equations are given by:

$$\bar{\rho} \frac{DK}{Dt} = a_j \frac{\partial \bar{p}}{\partial x_j} + \frac{\partial}{\partial x_j} \left(\frac{\mu_T}{\sigma_k} \frac{\partial K}{\partial x_j} \right) - R_{ij} \frac{\partial \tilde{u}_i}{\partial x_j} - \bar{\rho} \frac{K^{3/2}}{L} \quad (8)$$

$$\begin{aligned} \bar{\rho} \frac{DL}{Dt} = \frac{L}{K} \left[\left(\frac{3}{2} - C_4 \right) a_j \frac{\partial \bar{p}}{\partial x_j} - \left(\frac{3}{2} - C_1 \right) R_{ij} \frac{\partial \tilde{u}_i}{\partial x_j} \right] \\ - C_3 \bar{\rho} L \frac{\partial \tilde{u}_j}{\partial x_j} + \frac{\partial}{\partial x_j} \left(\frac{\mu_T}{\sigma_L} \frac{\partial L}{\partial x_j} \right) - \left(\frac{3}{2} - C_2 \right) \bar{\rho} K^{1/2} \end{aligned} \quad (9)$$

$$\bar{\rho} \frac{Da_i}{Dt} = b \frac{\partial \bar{p}}{\partial x_i} + \bar{\rho} \frac{\partial a_i a_j}{\partial x_j} - \bar{\rho} a_j \frac{\partial \tilde{u}_i - a_i}{\partial x_j} - \frac{R_{ij}}{\bar{\rho}} \frac{\partial \bar{\rho}}{\partial x_j} + \frac{\partial}{\partial x_j} \left(\frac{\mu_T}{\sigma_a} \frac{\partial a_i}{\partial x_j} \right) - C_a \bar{\rho} a_i \frac{K^{1/2}}{L} \quad (10)$$

$$\bar{\rho} \frac{Db}{Dt} = 2\bar{\rho} a_j \frac{\partial b}{\partial x_j} - 2(b+1)a_j \frac{\partial \bar{\rho}}{\partial x_j} + \bar{\rho}^2 \frac{\partial}{\partial x_j} \left(\frac{\mu_T}{\bar{\rho}^2 \sigma_b} \frac{\partial b}{\partial x_j} \right) - C_b \bar{\rho} \frac{K^{1/2}}{L} b \quad (11)$$

The turbulence equations must now be coupled back to the bulk hydrodynamics. The Reynolds stress term in the momentum equation is closed using the algebraic relation:

$$R_{ij} = 2/3 \bar{\rho} K \delta_{ij} - 2\sigma_1 \mu_T S_{ij} \quad (12)$$

with the additional definition:

$$S_{ij} = \frac{1}{2} \left[\frac{\partial \tilde{u}_i}{\partial x_j} + \frac{\partial \tilde{u}_j}{\partial x_i} - \frac{2}{3} \frac{\partial \tilde{u}_k}{\partial x_k} \delta_{ij} \right]$$

Note here that although Ref. [7] includes a more elaborate approximation for the Reynolds stresses, the validation cases in the present work use the above form to close the Reynolds stresses. Future work will include the additional terms for accurately capturing RM instabilities.

The turbulent-mass-flux term in the species-concentration equation is closed using a gradient-diffusion approximation:

$$\overline{\rho c_k'' u_j''} = -\frac{\mu_T}{\sigma_c} \frac{\partial \tilde{c}_k}{\partial x_j}$$

Relating this term to a species drift velocity gives:

$$u_{dk,j} = \frac{-\mu_T}{\rho \tilde{c}_k} \frac{\partial \tilde{c}_k}{\partial x_j} \quad (13)$$

this drift velocity definition is necessary to utilize the advection machinery in FLAG.

Finally the coupling of the turbulence to the energy equation requires some care. First, we add the dissipation from the K equation. This is not found naturally in the bulk equations due to lack of viscosity. However, it is included in the BHR equation for K . Physically this represents irreversible loss of turbulent kinetic energy to heat, and thus must be included (with opposite sign) in the energy equation. Second, the mean velocity in the work term is split into the mass-weighted velocity and the mass-flux velocity.

Third, the turbulent energy diffusion, $\overline{\rho e'' u_j''}$, must be modeled. A gradient-diffusion model that approximated this term as $\sim \mu_T \nabla \tilde{e}$ could be used[7]. However, the underlying multi-component behavior suggests an alternative closure. The specific internal energy of the bulk can be written as the sum of the internal energy of components

$$e = \sum c_k e_k = \sum \tilde{c}_k \tilde{e}_k + \tilde{c}_k e_k'' + \tilde{e}_k c_k'' + e_k'' c_k'' \quad (14)$$

Now writing the turbulent energy flux (substituting e for e'') gives:

$$\overline{\rho e u_j''} = \sum \tilde{c}_k \overline{\rho e_k'' u_j''} + \tilde{e}_k \overline{\rho c_k'' u_j''} + \overline{\rho c_k'' e_k'' u_j''} \quad (15)$$

The first term on the right-hand side can be simplified by noting that the for the cases of present interest the materials are in pressure/temperature equilibrium. Thus:

$$e_k = c_{v,k} T \quad (16)$$

Under the assumption that $c_{v,k}$ is a weak function of temperature (i.e. it changes more slowly than temperature), the fluctuations in e_k can be attributed to fluctuations in temperature. Applying the gradient diffusion approximation gives:

$$\sum \tilde{c}_k \overline{\rho e_k'' u_j''} = \sum \tilde{c}_k c_{v,k} \overline{\rho T'' u_j''} = -c_v \frac{\mu_T}{Pr_T} \frac{\partial \tilde{T}}{\partial x_j} \quad (17)$$

This term is commonly found in many single-fluid turbulence models.

The second term on the right-hand side represents the movement of species energy based on the turbulent mass flux. In FLAG this is handled naturally as the advection process that moves mass advects specific internal energy also. Some authors[16] suggest that when mass is diffused species enthalpy ($h_k = e_k + p_k/\rho_k$) must be diffused as well. In BHR-2, the treatment of a_i in the energy equation accounts for this effect (see Appendix A).

This gives the final form for the bulk equations in the FLAG implementation of BHR-2:

$$\frac{D\bar{\rho}}{Dt} = -\bar{\rho} \frac{\partial \tilde{u}_j}{\partial x_j} \quad (18)$$

$$\bar{\rho} \frac{D\tilde{c}_k}{Dt} = \frac{\partial}{\partial x_j} \frac{\mu_T}{\sigma_c} \frac{\partial \tilde{c}_k}{\partial x_j} \quad (19)$$

$$\bar{\rho} \frac{D\tilde{u}_i}{Dt} = -\frac{\partial}{\partial x_j} (\bar{p} \delta_{ij} + R_{ij}) + \bar{\rho} g_i \quad (20)$$

$$\bar{\rho} \frac{D\tilde{e}}{Dt} = -\bar{p} \frac{\partial \tilde{u}_j}{\partial x_j} + \bar{p} \frac{\partial a_j}{\partial x_j} + \frac{\partial}{\partial x_j} \left(\frac{c_v \mu_T}{Pr_T} \frac{\partial \tilde{T}}{\partial x_j} \right) + \sum_k \frac{\partial}{\partial x_j} \left(\frac{\mu_T}{\sigma_c} \frac{\partial \tilde{c}_k}{\partial x_j} \tilde{e}_k \right) + \bar{\rho} \frac{K^{3/2}}{L} \quad (21)$$

With an equation of state that gives $\bar{p} = \bar{p}(\bar{\rho}, \tilde{T})$

B. Numerical Implementation in FLAG

Variable Organization

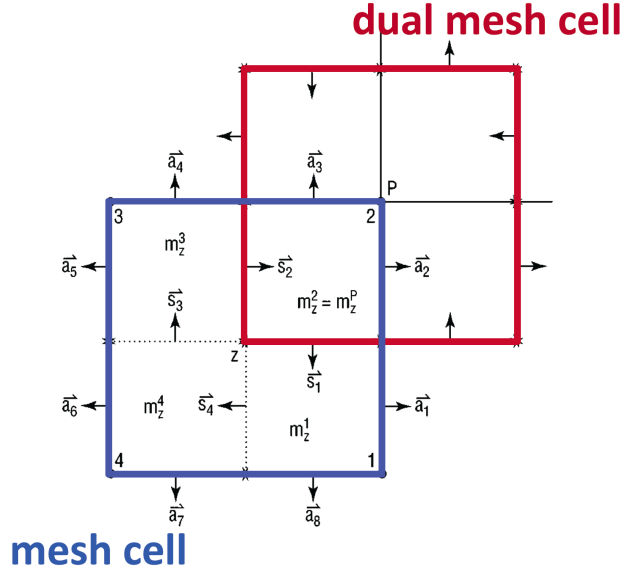


FIG. 1: Staggered Grid Layout[11], Velocities are stored on Points (P), Scalars stored on Zones (Z).

The scalar turbulence variables, K , L , and b are stored in mesh zones, the mass-flux velocity a_i is stored on points (See Figure 1). This allows for easily integrating the dissipation of turbulent kinetic energy (K) into the mean energy equation, which is stored on zones. Similarly, the pdV work contribution from a_i in the energy equation can be treated

consistently with the velocity field which is stored on points. The vector calculus operations (divergence, gradient) are computed using standard finite volume techniques found in FLAG.

Codeflow

The turbulence model is integrated into the code using a four-stage, low-storage, Runge-Kutta algorithm and splits the species mixing into two half-steps surrounding the bulk hydro and mix-model evolution[10]. For the present work, all computations assume pressure and temperature equilibrium among the species. This is done by computing equilibrium volume fractions α_i after each mixing step. This results in a sequence of steps:

1. Species mixing for $\Delta t/2$
2. P/T equilibration
3. Bulk hydrodynamic evolution for Δt using predictor-corrector
4. Mix-model evolution for Δt using Runge-Kutta
5. Species mixing for $\Delta t/2$
6. P/T equilibration
7. Mesh relaxation/remapping

Species Advection

In addition to the bulk advection, the turbulence model leads to species advection using the drift velocity defined by Eq. 13. The species mixing is evaluated and limited in the same manner as the bulk hydrodynamics in FLAG, i.e. using an FCT-based scheme[12]. An additional check is necessary to enforce conservation of total mass in a zone during this process, after the species flux are computed and limited the incoming and outgoing mass flux may not sum to zero. To enforce mass conservation, the minimum of the incoming and outgoing flux is used.

Numerical Limiters

As part of the implementation process for BHR in the Eulerian code xRAGE[17], several numerical limiters were put in place to ensure robustness. In FLAG, the primary limits that must be set are a minimum value for K , a minimum value for L , a maximum value for L , and a cutoff value for b ($b = 0$ if $b < \text{cutoff}$). The cutoff value for b is set to $1\text{e-}6$ as per Ref. [7], and must be reduced to approximately machine precision for low Atwood number cases.

In addition to limiting the turbulence parameters, the turbulent kinetic energy in the denominator of L/K in the L equation is limited to the initial value of turbulent kinetic energy $K = \max(K(0), K)$. This prevents very small values of K from generating large production of L . Future work should revisit the necessity of these limiters. They are necessary in FLAG to reproduce the xRAGE behavior, but do not appear to be necessary for numerical reasons.

See the code documentation for how to set and disable these limiters.

Boundary Conditions

The present implementation enforces the same boundary conditions on the mass-flux velocity (a_i) as the bulk velocity. Work is ongoing to improve the boundary conditions at multi-material (non-mixing) interfaces.

C. Parameter Values and Initial Conditions

There are many parameters in the BHR model that are set from canonical test cases. The source of these terms can be found in several places[7, 13]. The default model coefficients for the present work are summarized in Table I.

Pr_T	σ_c	C_1	C_2	C_4	σ_L	C_a	σ_a	C_b	σ_b	C_μ
1.0	0.6	1.44	1.92	1.05	0.1	6.0	1.0	3.0	2.5	0.28

TABLE I: Default Parameter Values for BHR

Initialization of any turbulence model from a steady initial condition is a challenge as

the models assume developed, turbulent flow. The model is initialized with zero mass-flux velocity ($a_i = 0$), the density-specific volume correlation zero everywhere except cells that are initially mixed, where it is set to the two-fluid incompressible value. The initial conditions that require investigation are the initial turbulent length scale and kinetic energy.

Prior work indicates good results are achieved by setting the initial length scale to the most amplified wavelength from linear stability analysis[7]. If this is not known, a fraction of the grid spacing can be used. Ref. [7] recommends setting K using:

- **Kelvin–Helmholtz:** $K = 0.01(U_2 - U_1)^2$
- **Rayleigh–Taylor:** $K = 0.01AgL_0$
- **Richtmyer–Meshkov:** $K = 0.01[u]^2$

Work is ongoing to improve the initialization of the BHR model to remedy these ad-hoc initializations[18].

III. HOMOGENEOUS TEST PROBLEMS

The decay of homogeneous isotropic turbulence is used to set the coefficient C_2 . In this case the equations reduce to:

$$\frac{dK}{dt} = -\frac{K^{3/2}}{L}; \quad \frac{dL}{dt} = -\left(\frac{3}{2} - C_2\right) \sqrt{K}$$

The procedure to find C_2 is outlined in standard turbulence texts[19], briefly, assume solutions of the appropriate form:

$$K = K_0 \tau^{-a}; \quad L = L_0 \tau^{-b}$$

where $\tau = t/t_0$, and substitute to obtain:

$$\frac{K_0}{t_0} a \tau^{-a-1} = \frac{K_0^{3/2}}{L_0} \tau^{-3a/2+b} \quad (22)$$

$$\frac{L_0}{t_0} b \tau^{-b-1} = \left(\frac{3}{2} - C_2\right) K_0^{1/2} \tau^{-a/2} \quad (23)$$

The exponents give: $a = 2b + 2$, and the coefficients give $b = \left(\frac{3}{2} - C_2\right) a$, solving for C_2 gives:

$$C_2 = 1 + \frac{1}{a} \quad (24)$$

Ref. [7] follows the standard $k - \epsilon$ model to set the decay rate, $a = 1.09$, which gives $C_2 = 1.92$. Figure 2 shows that FLAG is able to accurately capture this decay starting with $K = 1$ and $L = 0.1$.

The idea of isotropic decay can be extended to include the effects of a constant pressure gradient, and validate the chief production terms in BHR. Assuming homogeneous fields and constant b , the BHR equations reduce to:

$$\rho \frac{DK}{Dt} = a \frac{\partial p}{\partial x} - \rho K^{3/2}/L \quad (25)$$

$$\rho \frac{DL}{Dt} = \frac{L}{K} \left(\frac{3}{2} - C_4\right) a \frac{\partial p}{\partial x} - \left(\frac{3}{2} - C_2\right) \rho K^{1/2} \quad (26)$$

$$\rho \frac{Da}{Dt} = b \frac{\partial p}{\partial x} - C_a \rho a K^{1/2}/L \quad (27)$$

These equations can be integrated numerically as ODEs and compared to results in FLAG. Figure 3 shows the homogeneous evolution with a constant value $b = 0.01$, and initial values: $a = 0$, $K = 1$, and $L = 0.1$.

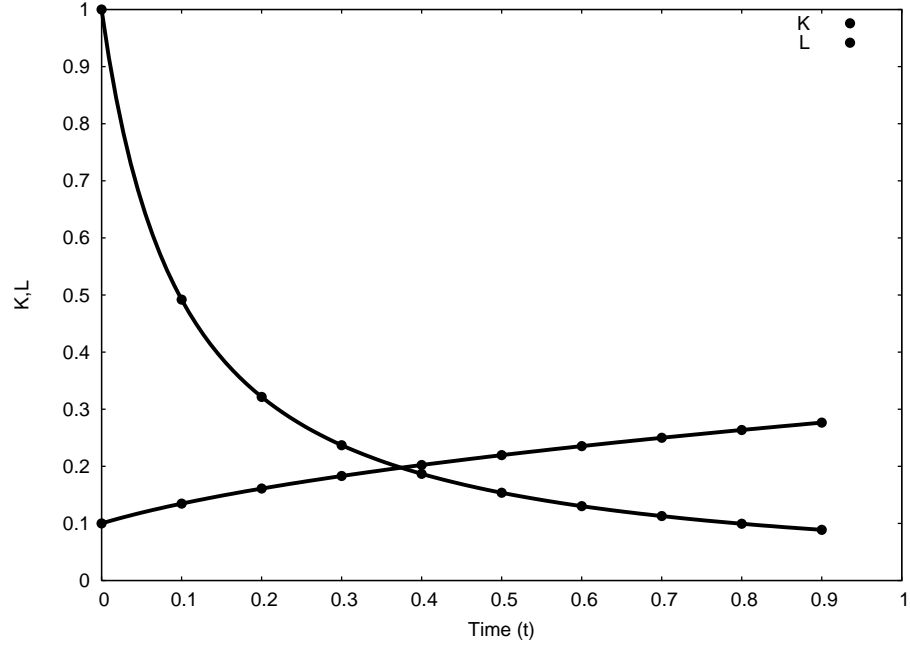


FIG. 2: Isotropic Decay in FLAG comparing theory (lines) and computation (points)

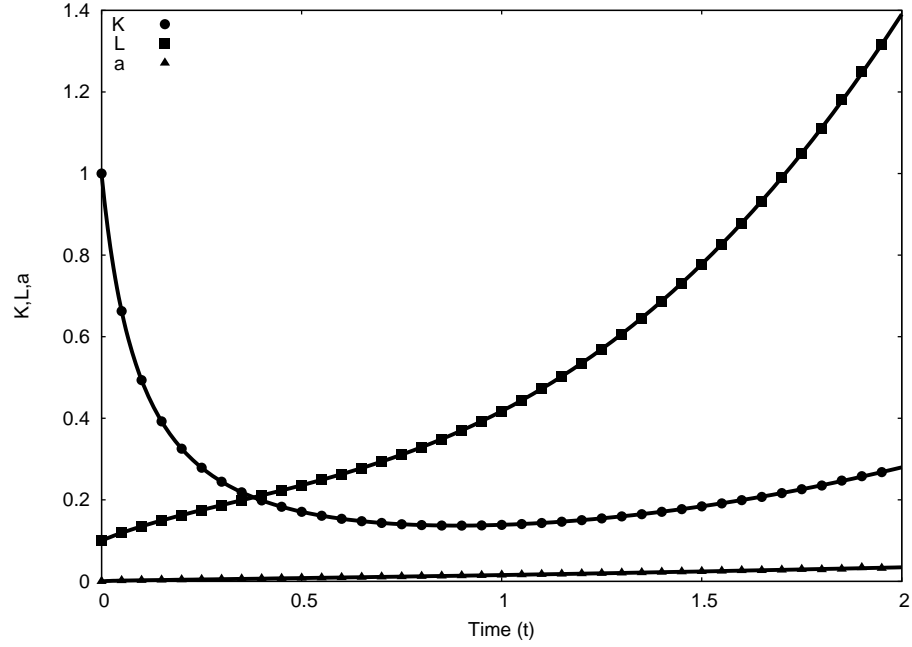


FIG. 3: Homogeneous Evolution in FLAG comparing ODEs (lines) and full computation (points)

IV. RAYLEIGH–TAYLOR VALIDATION

One of the primary motivations for the BHR family of models is capturing turbulent mixing due to unstable density stratification. The canonical example of these flows is the Rayleigh–Taylor Instability. Here, a heavy fluid is placed above a light fluid under the influence of gravity. This arrangement is unstable and the two fluids begin to mix as the flow evolves. Fully capturing the growth of the mixing layer requires 3D direct numerical simulations (DNS) which is not practical for many applications. Monotone Integrated Large Eddy Simulation (MILES) has proved to be successful for these types of flows[20], but also requires 3D simulations at relatively high resolution. The goal of the BHR model is to simulate the mean behavior in an efficient way, allowing it to be used in multi-physics contexts.

The present work looks at three validation cases. Two are canonical 1D mean flows, differing only in their Atwood number ($A_t = (\rho_H - \rho_L)/(\rho_H + \rho_L)$). The third is a 2D mean flow with both mixing and bulk hydrodynamic effects. The discussion here is not meant to be scientifically exhaustive, but merely to demonstrate the model implementation in comparison to previous work. Specifically, comparisons will be made to the Eulerian code xRAGE[17] where the BHR model was initially developed and validated.

The features of interest in the 1D simulation are the profiles of the mixing layer, as well as the asymptotic values once in the self-similar regime. Let α be the expected asymptotic amplitude. We have from theory[7]:

$$\begin{aligned}\alpha &= \frac{\Delta h}{\Delta A_t g t^2} \\ \alpha_K &= \frac{\Delta \max(K)}{\Delta (A_t g t)^2} \\ \alpha_a &= \frac{\Delta \max(a)}{\Delta A_t g t} \\ \alpha_L &= \frac{\Delta \max(L)}{\Delta A_t g t^2} \\ \alpha_b &= \max(b)\end{aligned}$$

Where Δ is the change in the quantity, h is defined as distance between 5% and 95% of the density profile, and maximums are taken over the entire domain. As the flow approaches self similarity (regardless of initial conditions) these numbers should tend to known constants.

A. 1D Moderate Atwood Number

The first case of interest is used for comparison to Ref. [7]. The parameters are given in Table II.

ρ_H	ρ_L	K_0	L_0	P_0	T_0	n_x	L_x	g	γ
3.0	1.0	0.10	0.01	1e7	300	400	400	1000	1.4

TABLE II: Moderate A_t Simulation Conditions, all units cgs with temperature in K

The simulation starts with an initially sharp interface and evolves to a self similar state where the profiles can be evaluated. Figure 4 shows the convergence of the different turbulence variables.

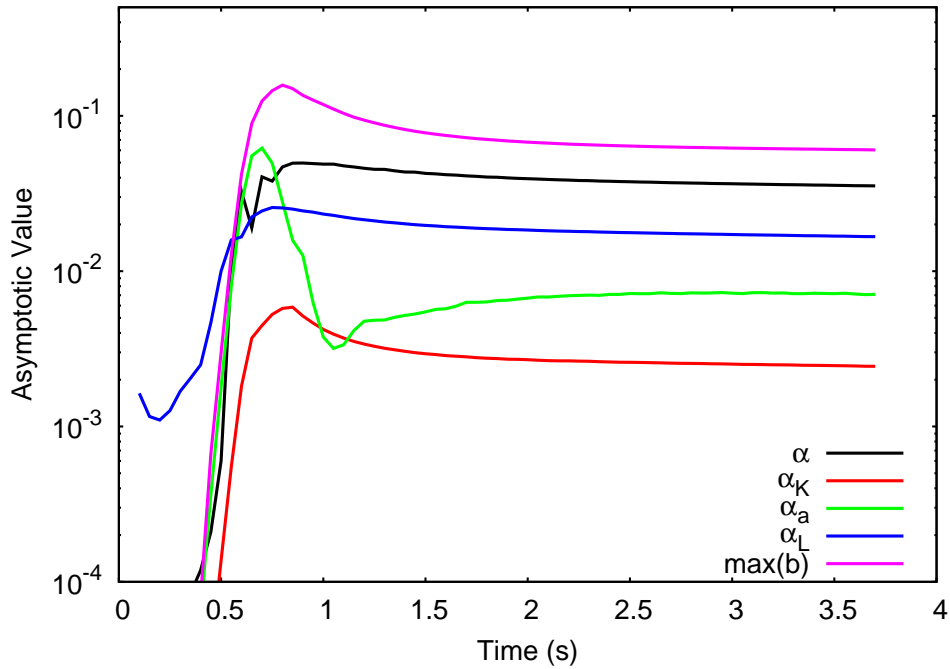


FIG. 4: Convergence to self similar behavior

At $t = 3.7$ the results have mostly converged, and are compared to the results reported in Ref. [7]. Table III shows that FLAG is comparable to xRAGE and the DNS, falling between the two results for the overall growth of the mixing layer as well as the turbulent kinetic energy. FLAG is lower than both RAGE and the DNS for the mass flux growth rate. This appears to be a result of greater species mass flux in the mass-fraction equations. When

Parameter	DNS	FLAG	xRAGE
α	0.035	0.0354	0.0359
α_k	0.0024	0.0024	0.0026
α_a	0.0108	0.0071	0.0083

TABLE III: Growth rates from DNS, xRAGE and FLAG

the turbulent Schmidt number (σ_c) is raised, a higher value of α_a and lower value of α_K are found. This difference will also be seen in the low Atwood number case where it is relevant to capturing the correct density profile. This is likely an difference in code implementation as each code has different methods for fluxing and limiting species mass transfer.

The volume fraction across the mixing layer is one of the key variables in the mixing model. At low A_t this profile is nearly linear, but it is curved for moderate density ratios. Figure 5 compares the volume fraction of the heavier fluid as a function of x for xRAGE and FLAG. The agreement is very good. Additionally the Lagrangian nature of FLAG can be seen as the initial evenly spaced grid moves with the mass-averaged velocity \tilde{u} .

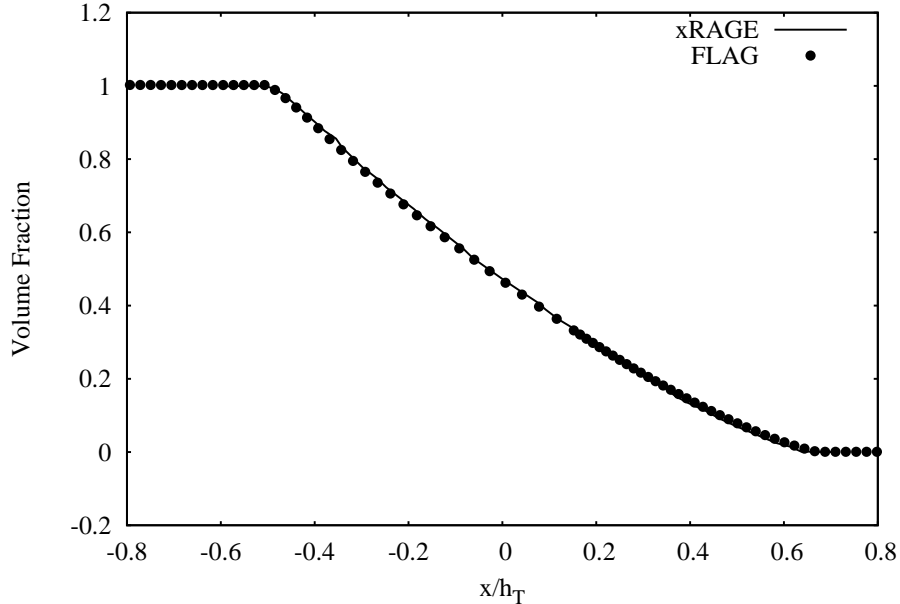


FIG. 5: Volume Fraction of Heavy Fluid

A more detailed comparison between FLAG and xRAGE results can be found from a term-by-term comparison of the driving mechanisms in the transport equation. Plotting all

the dominant terms as a function of mix width, Figure 6 shows the Pressure Production ($a_i \partial p / \partial x_i$), Reynolds stress production, diffusion, and dissipation terms. (Note the axes have been flipped from Ref. [7] because gravity is positive in the present simulations, and the Reynolds stress term from xRAGE has been divided by three here and in the a equation plots to account for post-processing differences).

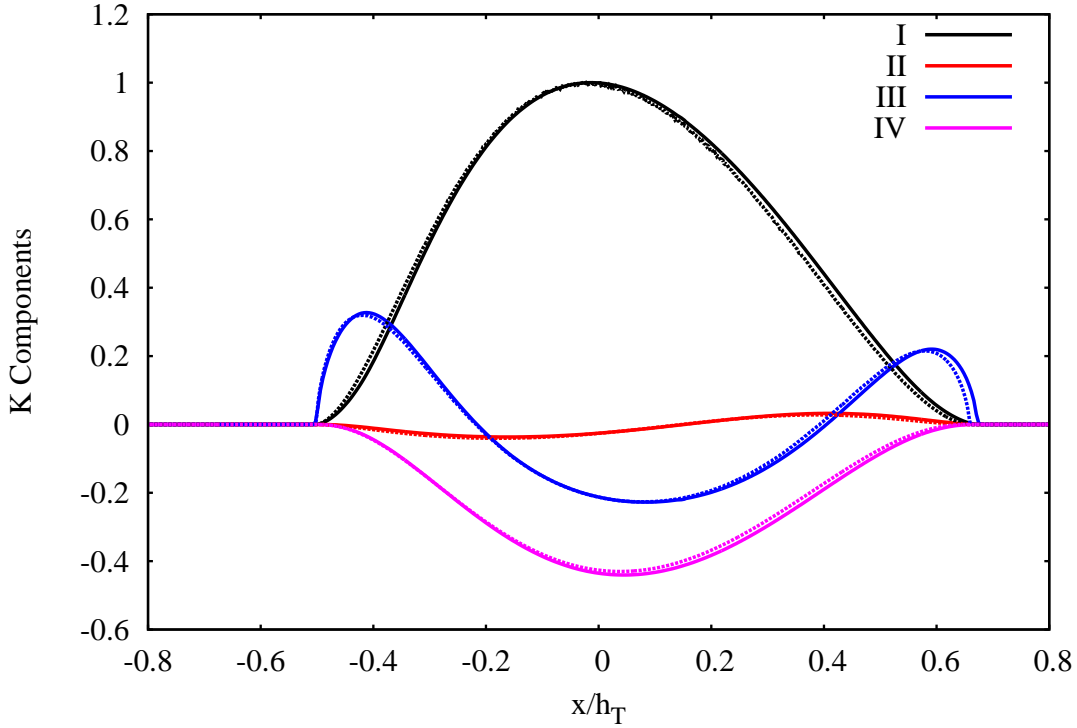


FIG. 6: Term Comparisons in the K equation for FLAG (solid) and xRAGE (dashed), I: Pressure Production, II: Reynolds Stress Production, III: Diffusion, IV: Dissipation

Figure 7 shows a similar plot for the terms in the mass-flux velocity equation, with the pressure production ($b \partial p / \partial x_i$) again the dominant term. These two figures show excellent agreement between FLAG and xRAGE on the most important terms in the BHR turbulence model.

The only differences can be found in Figure 8 which plots the terms from the b equation. The diffusion operator (III in blue) shows unphysical spikes at the edges of the mixing layer. This is not unheard of, xRAGE sees these features in the length scale equation, but in FLAG these features appear due to the cutoff value in the b equation and disappear if this limiter is removed (though this changes the growth rates). Future work should address the necessity

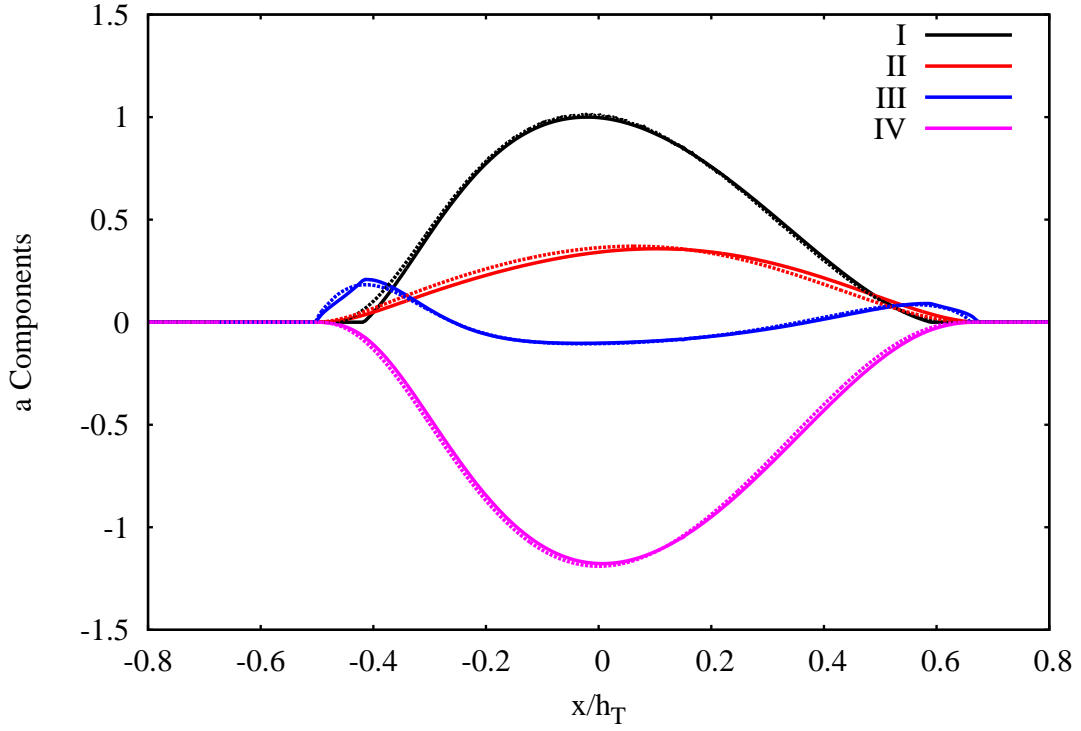


FIG. 7: Term Comparisons in the a equations for FLAG (solid) and xRAGE (dashed), I: Pressure Production, II: Reynolds Stress Production, III: Diffusion, IV: Dissipation

of this additional limiter. Further, since the computation of the b equation components in xRAGE was done as a post-processing step, whereas in FLAG the data is output directly, it may simply be the difference in how the gradients are computed.

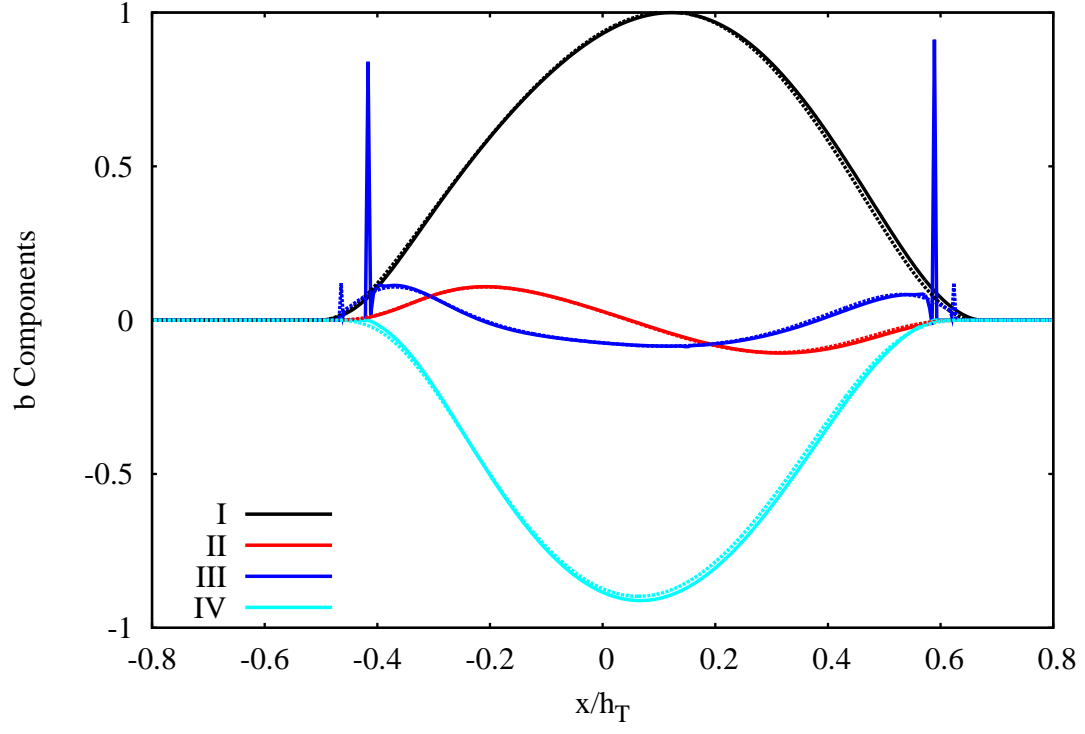


FIG. 8: Term Comparisons in the b equation for FLAG (solid) and xRAGE (dashed), I: Density Gradient Production, II: b Gradient Production, III: Diffusion, IV: Dissipation (all divided by ρ)

B. 1D Low Atwood Number

Low Atwood number flows are a useful test case because close comparisons can be made to semi-analytic solutions[13]. These cases are also sensitive to the species mass transport and compressibility effects because the density differences are so small.

The case considered here is based on the experiments in the Texas A&M gas channel, with an Atwood number $A_t = 0.04$ [21]. All conditions are the same as the moderate Atwood number simulations, except the initial turbulent length scale and turbulent kinetic energy are increased by a factor of ten, and $C_3 = 0.75$, consistent with Ref. [13].

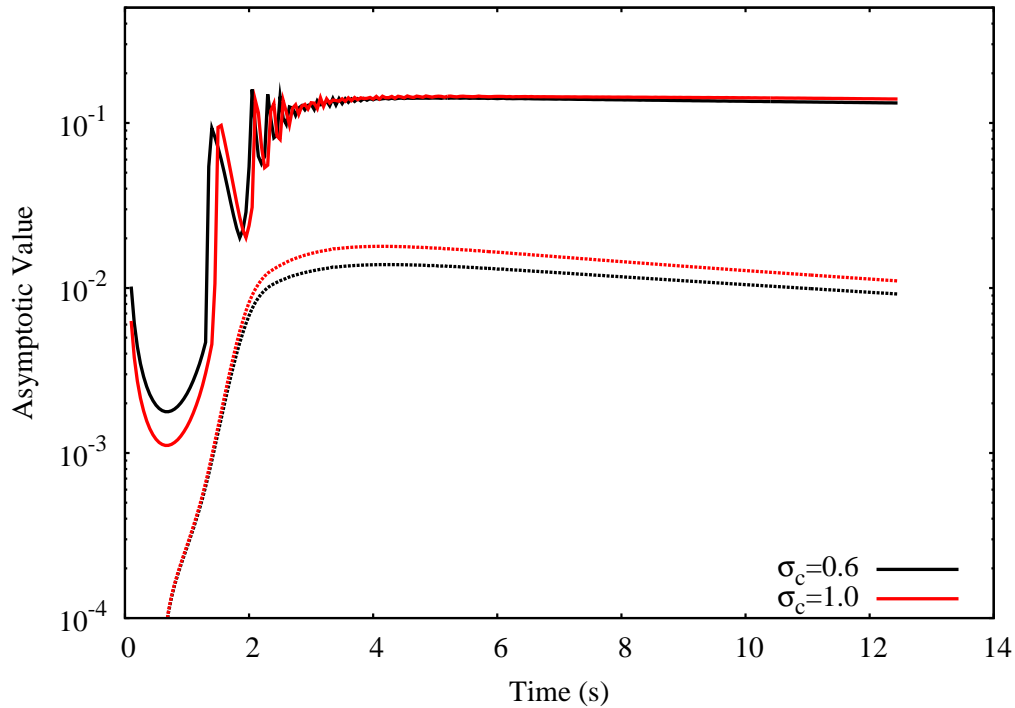


FIG. 9: Approximately self-similar behavior in FLAG for α (solid) and α_K (dashed)

Initialized from a sharp interface, the low A_t cases take longer to converge, but Figure 9 shows an approximately self-similar profile is reached with $\alpha = 0.135$ at $t = 10$. The asymptotic value for the mix width agrees well with previous results, again falling in between the xRAGE result of 0.13 and the experimental result of 0.14. There is still some decay in K happening (similarly in a_i , not shown) but this is relatively small and similar to the error bars in Ref. [7].

As mentioned above, the primary implementation difference between FLAG and xRAGE

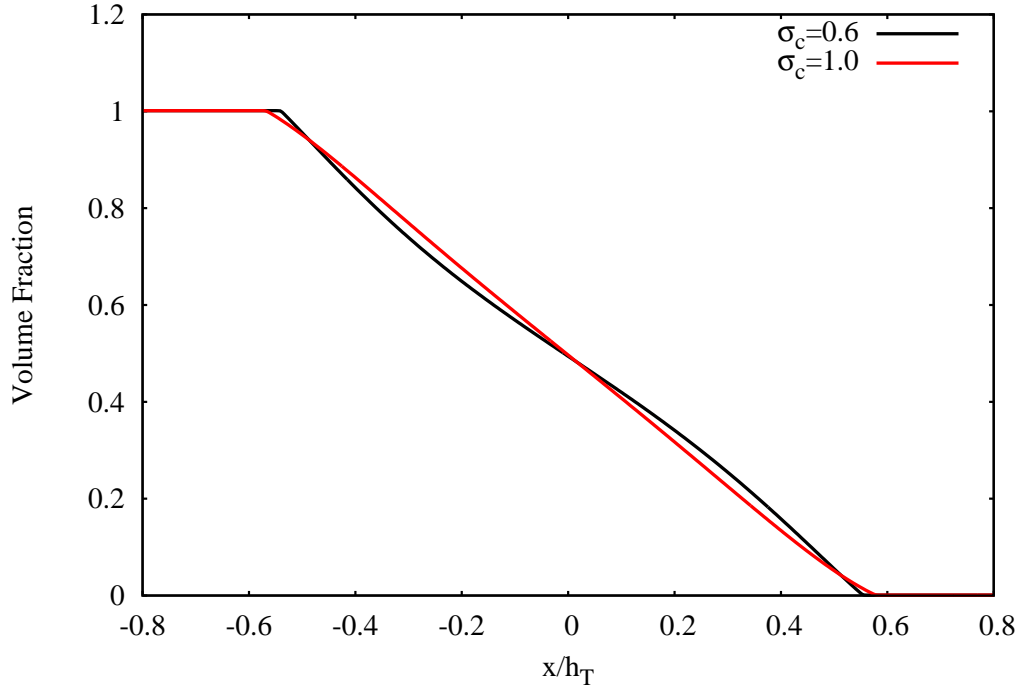


FIG. 10: Volume Fraction Profiles

is the treatment of the species mass flux. The current work suggests that more species mass is moved by FLAG than by xRAGE, i.e. FLAG is more diffusive. This is seen in the moderate A_t case as a lower mass flux velocity. In the low A_t case it is seen clearly in the volume fraction profiles. The self-similar profile ought to be nearly linear, but using the standard xRAGE parameters we see a slightly “S” shaped profile in Figure 10.

This can be mitigated in two ways either by increasing the turbulent Schmidt number or increasing the static pressure. Changing the Schmidt number solves the problem directly by simply diffusing less mass. This also brings the mass-flux velocity in line with the mass-averaged velocity ($a_i \approx \tilde{u}_i$) which is expected for low A_t flows, and $\sigma_c = 1$ is the analytical self-similar value. Increasing the static pressure is less intuitive, but may work via the coupling of species internal energy to the pressure field. Increasing the static pressure forces the profile to be more flat, but accelerates the mixing layer growth. This behavior is not ideal, and motivates future work on detailed parameter studies.

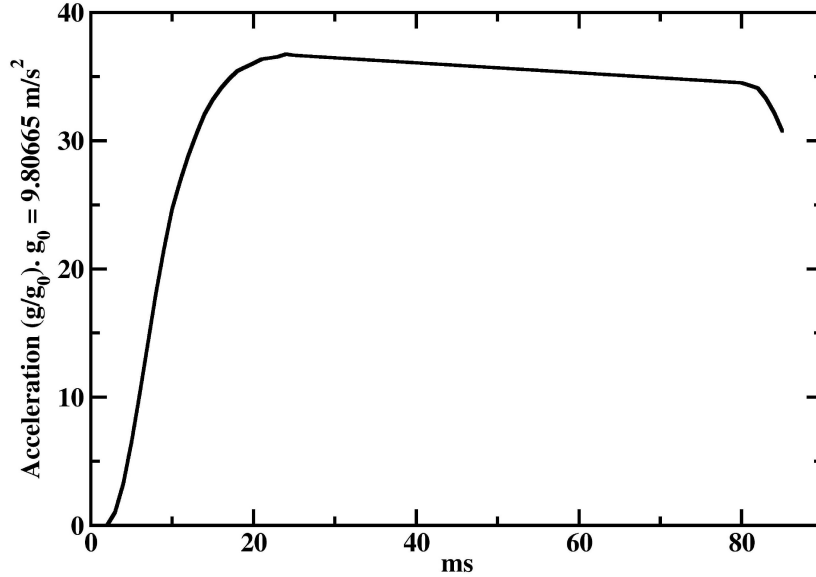


FIG. 11: Acceleration profile from Ref. [22]

C. 2D Tilt Rig

The tilted rig experiment[22] was part of a series of experiments performed at AWE investigating turbulent mixing via the Rayleigh–Taylor instability. In these experiments heavy fluid was placed in a tank below light fluid (a stable configuration). Rocket motors fired, accelerating the tank downward effectively changing the direction of “gravity” so that the system was RT unstable. The acceleration was documented, and images were taken of the growing mixing layer.

The tilted rig was a variation on this experiment where the initial tank was at an angle relative to gravity, and when the rockets fired the acceleration was not perpendicular to the interface. This results in both RT mixing and a bulk overturning motion in the fluid. The present work uses this case to validate the BHR model in cases where these two-dimensional effects are present.

This problem has been studied by Smeeton & Youngs [22], Andrews & Spalding [20, 23], Ptitzyna *et al.* [24], Rollin & Andrews [25] and Wei & Livescu [26]. Detailed comparison of FLAG results to DNS and LES can be found in Ref. [27], only some qualitative features will be presented here to demonstrate the model capabilities.

The test problem shown here is Case 110 from Ref. [22]. For this problem, $\rho_H = 1.89$ g/cm³, and $\rho_L = 0.66$ g/cm³ (the fluids are NaI and hexane respectively). This gives an

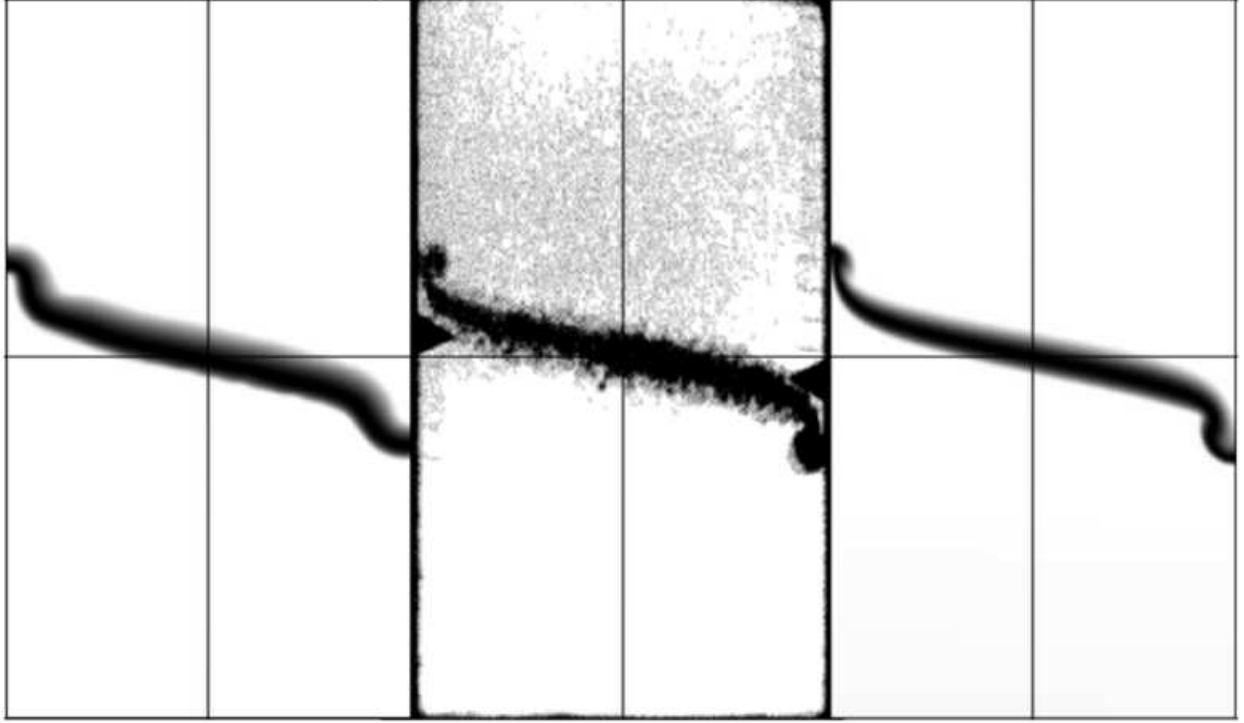


FIG. 12: Mix region from xRAGE (left), Experiment (center), and FLAG (right). Interface visualized by $4\alpha_1\alpha_2$ at $t=36$ ms

Atwood number, $A_t = 0.48$. The acceleration from the rocket motors was not constant, and is shown in Figure 11. The initial tilt was 5.77° which leads to significant overturning motion in addition to the turbulent mixing. The goal of the present work is to show how well the turbulence models, which were validated using canonical test cases, perform with the additional complications presented by the two-dimensional interface.

The simulations were performed on square grids, with 150×240 grid points in a domain $15 \text{ cm} \times 24 \text{ cm}$. The interface pressure and temperature are set to minimize compressibility effects, in FLAG the densities were increased by a factor of a thousand to be in units of kg/m^3 , the interface pressure was set at $1e5 \text{ Pa}$, and the temperature set to 300K . The initial length scale was set based on an estimate of the most amplified wavelength from linear theory, 0.1 mm , and the initial kinetic energy is set using the guidelines given above.

Figure 12 shows the mix width at a relatively early time by visualizing the product of the volume fractions α_i . The thickness here is comparable between both codes and the experiment. FLAG seems to capture the asymmetry between the bubble (right) and spike (left) of the image better than xRAGE.

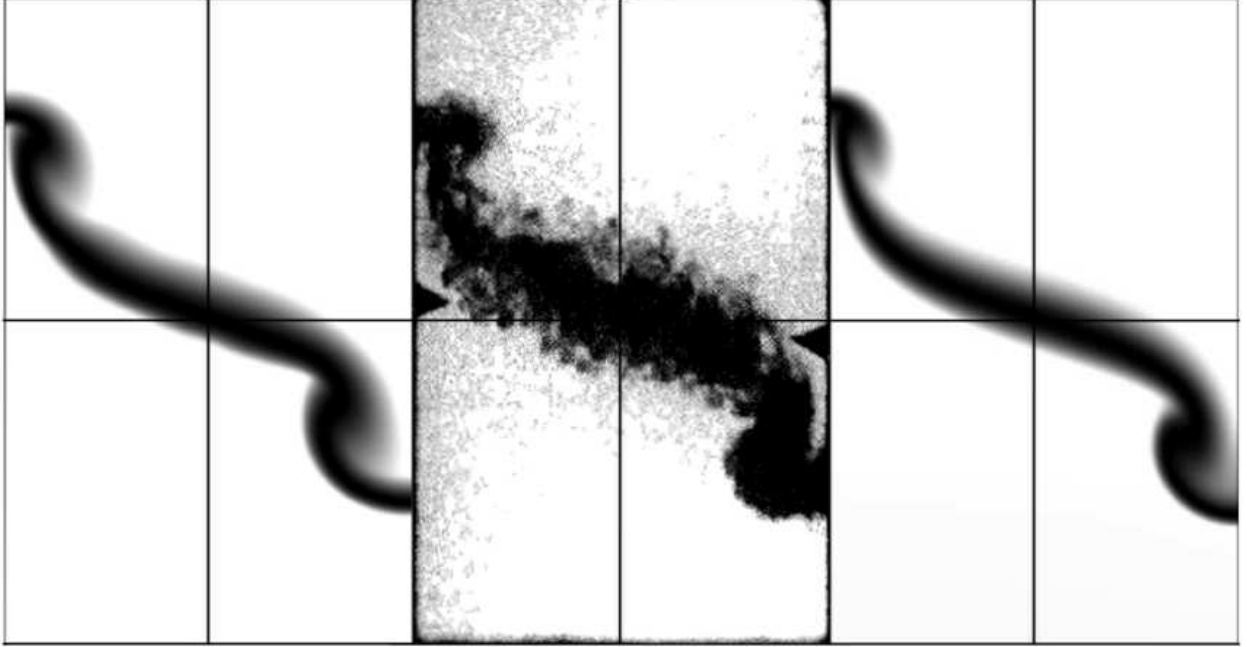


FIG. 13: Mix region from xRAGE (left), Experiment (center), and FLAG (right). Interface visualized by $4\alpha_1\alpha_2$ at $t=55$ ms

Figure 13 shows a snapshot of the mix width at later time. The codes do a good job of predicting the heights of the evolving spike and bubble as well as the overturning motion of the mixing layer. This is shown quantitatively in Figure 14 for two different FLAG resolutions as well as xRAGE and the experiments. The growth of the center mix region seems somewhat under-predicted. More detailed comparison of the turbulence quantities can be found elsewhere[25].

V. CONCLUSIONS AND FUTURE WORK

This report gave a description of the BHR implementation in the FLAG hydrocode. Detailed comparison with the implementation in xRAGE were presented that demonstrated FLAG's ability to reproduce some of the canonical Rayleigh–Taylor results. In the process, some differences were highlighted that should be targets for future work. Most importantly, the existence of two non-physical limiters, the floor on the b equation, and the maximum value of K in the denominator of the L equation should be revisited. Work in FLAG indicates these terms may not be necessary, though their removal would require a recalibration of model constants.

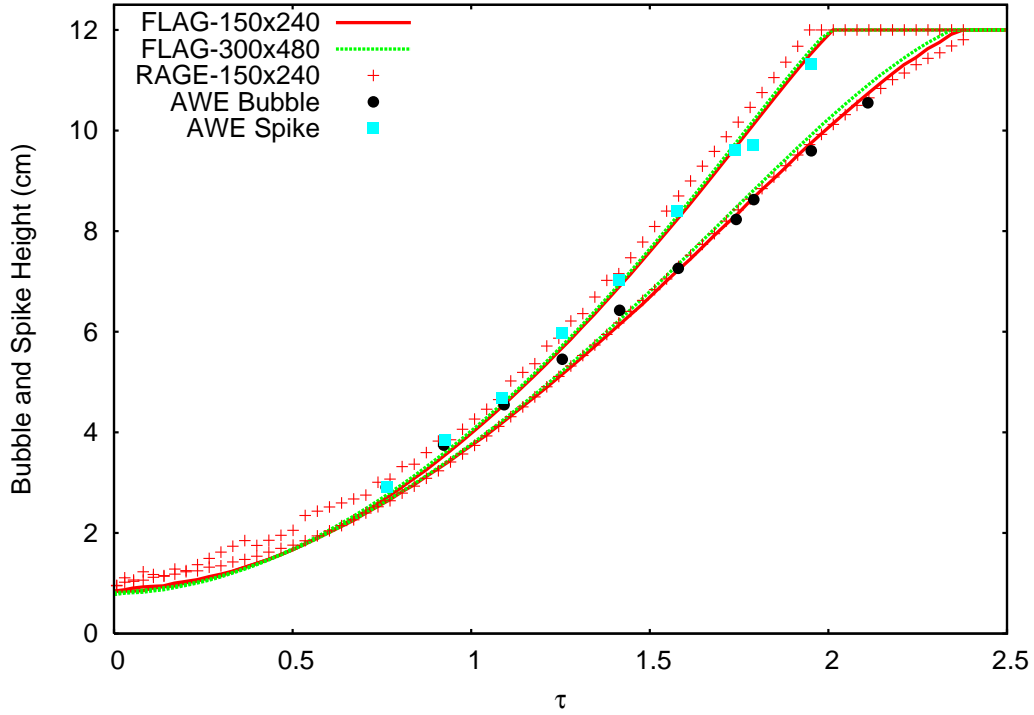


FIG. 14: Bubble and Spike evolution for FLAG, xRAGE and Experiment.

Additionally, especially in low A_t cases, the RT test problems seems sensitive to the amount of species mass that is moved. This results from the decoupling of turbulent species-mass flux ($\overline{\rho c_k'' u_i''}$) from the mass-flux velocity (a_i). The models for these two terms should be related, but are not in the current form of BHR. The difference in species-mass flux is also the most significant code implementation difference between FLAG and xRAGE, and a detailed parameter study involving both codes may be necessary to sort out all the mechanisms present.

Finally, xRAGE contains a realizable Reynolds stress model that is necessary to accurately capture the behavior of turbulence in the vicinity of shocks. This should be implemented in FLAG as soon as possible.

APPENDIX A: MULTI-SPECIES ENERGY DIFFUSION

The BHR turbulence model attempts to capture the behavior of variable density mixtures with as much fidelity as possible. One of the key features is the ability to relate multi-component descriptions of fluid flow to the BHR equations. This procedure provides some insight into closing the species mass and energy equations.

Let α_k , ρ_k , and c_k be the species volume fraction, density, and concentration. These are related by:

$$\alpha_k \rho_k = \rho c_k$$

with

$$\sum \alpha_k = \sum c_k = 1$$

Now the instantaneous, volume averaged, equations for multi-component flow can be written in terms of the species velocity, pressure and energy:

$$\frac{\partial}{\partial t} \alpha_k \rho_k + \nabla \cdot (\alpha_k \rho_k u_k) = 0 \quad (\text{A1})$$

$$\frac{\partial}{\partial t} \alpha_k \rho_k u_k + \nabla \cdot (\alpha_k \rho_k u_k u_k) = -\nabla \alpha_k p_k \quad (\text{A2})$$

$$\frac{\partial}{\partial t} \alpha_k \rho_k \left[e_k + \frac{u_k^2}{2} \right] + \nabla \cdot \left(\alpha_k \rho_k u_k \left[e_k + \frac{u_k^2}{2} \right] \right) = -\nabla \cdot (\alpha_k p_k u_k) \quad (\text{A3})$$

Now let $u_k = u + u_{dk}$ where u is the bulk and u_{dk} the drift velocity, and rewrite the species conservation equation in terms of concentration:

$$\frac{\partial}{\partial t} \rho c_k + \nabla \cdot (\rho c_k u) = -\nabla \cdot (\rho c_k u_{dk}) \quad (\text{A4})$$

The bulk velocity is defined such that, when summed over species: $\sum \rho c_k u_{dk} = 0$ and the bulk density equation is recovered:

$$\frac{\partial}{\partial t} \rho + \nabla \cdot (\rho u) = 0 \quad (\text{A5})$$

Using a similar substitution in the momentum equation gives

$$\frac{\partial}{\partial t} \rho c_k u + \frac{\partial}{\partial t} \rho c_k u_{dk} + \nabla \cdot (\rho c_k u u) + 2 \nabla \cdot (\rho c_k u_{dk} u) + \nabla \cdot (\rho c_k u_{dk} u_{dk}) = -\nabla \alpha_k p_k \quad (\text{A6})$$

Summing over species eliminates all the terms with $\rho c_k u_{dk}$, assuming the drift velocity is small compared to the bulk velocity eliminates the drift kinetic energy flux, and the bulk pressure is defined as $\sum \alpha_k p_k$, leaving the standard momentum equation:

$$\frac{\partial}{\partial t} \rho u + \nabla \cdot (\rho u u) = -\nabla p \quad (\text{A7})$$

From this equation we can form a mechanical energy equation as well:

$$\frac{\partial}{\partial t} \rho \frac{u^2}{2} + \nabla \cdot \left(\rho u \frac{u^2}{2} \right) = -u \cdot \nabla p \quad (\text{A8})$$

The energy equation is expanded and summed, ignoring terms of order u_{dk}^2 , and noting that the bulk energy is defined, $e = \sum c_k e_k$:

$$\frac{\partial}{\partial t} \rho \left[e + \frac{u^2}{2} \right] + \nabla \cdot \left(\rho u \left[e + \frac{u^2}{2} \right] \right) = -\nabla \cdot (pu) - \sum \nabla \cdot (\rho c_k u_{dk} e_k + \alpha_k p_k u_{dk}) \quad (\text{A9})$$

Subtracting the mechanical energy equation, and defining the species enthalpy $h_k = e_k + p_k/\rho_k$ gives the final form for the bulk energy equation in a multi-component mix:

$$\frac{\partial}{\partial t} \rho e + \nabla \cdot (\rho u e) = -p \nabla \cdot u - \nabla \cdot \left(\sum \rho c_k u_{dk} h_k \right) \quad (\text{A10})$$

The important thing to note from this derivation is the emergence of an enthalpy flux that is related to the species mass flux. That is, a given drift velocity, u_{dk} , will move both species mass (c_k) as well as species enthalpy (h_k). Thus far, aside from neglecting the drift kinetic energy, no modeling has been done. Frequently in multi-component formulations Fickian diffusion would be assumed, closing the equations via:

$$\rho c_k u_{dk} = -D \nabla c_k$$

Now the goal is to derive the turbulence model equations, neglecting miscibility, but keeping the multi-component formulation in mind in regards to closure modeling. Taking the average of the species equation gives:

$$\frac{\partial}{\partial t} \bar{\rho} \tilde{c}_k + \nabla \cdot (\bar{\rho} \tilde{c}_k \tilde{u}) = -\nabla \cdot (\overline{\rho c_k'' u''}) \quad (\text{A11})$$

In analogy to the diffusion assumption made in the multi-component case, the turbulent concentration-velocity correlation is treated like a diffusion term:

$$\overline{\rho c_k'' u''} = \rho \tilde{c}_k u_{dk} = -\mu_T \nabla \tilde{c}_k$$

As required, the sum of these diffusion terms over all species gives zero.

In analog to the multi-component case, multi-species effects do not enter the bulk momentum equation. However, these effects must be accounted for in the energy equation. The question is how to include them. If the goal was for the turbulent species diffusion to

behave as close to mass diffusion as possible, the multi-component formalism suggests one ought to move enthalpy in response to a flux of species mass. However, the details of the BHR derivation suggest that is not the case.

Consider two ways of writing the energy equation, neglecting miscibility, first as above:

$$\frac{\partial}{\partial t}\rho e + \nabla \cdot (\rho u e) = -p \nabla \cdot u \quad (\text{A12})$$

and second with the pressure term rewritten using the chain rule and absorbed into the energy advection:

$$\frac{\partial}{\partial t}\rho e + \nabla \cdot (\rho u h) = u \cdot \nabla p \quad (\text{A13})$$

We take an average of each equation to obtain

$$\frac{\partial}{\partial t}\bar{\rho}\tilde{e} + \nabla \cdot (\bar{\rho}\tilde{u}\tilde{e}) = -\overline{p\nabla \cdot u} - \nabla \cdot (\overline{\rho u''e''}) \quad (\text{A14})$$

and similarly

$$\frac{\partial}{\partial t}\bar{\rho}\tilde{e} + \nabla \cdot (\bar{\rho}\tilde{u}\tilde{h}) = \overline{u \cdot \nabla p} - \nabla \cdot (\overline{\rho u''h''}) \quad (\text{A15})$$

from the definition of enthalpy we have:

$$\bar{\rho}\tilde{h} = \bar{\rho}\tilde{e} + \bar{p}$$

and so can split the enthalpy equation to give the same left hand side

$$\frac{\partial}{\partial t}\bar{\rho}\tilde{e} + \nabla \cdot (\bar{\rho}\tilde{u}\tilde{e}) = \overline{u \cdot \nabla p} - \nabla \cdot (\tilde{u}\bar{p}) - \nabla \cdot (\overline{\rho u''h''}) \quad (\text{A16})$$

and splitting the pressure-velocity terms, and using $\bar{u} = \tilde{u} - a$ gives:

$$\frac{\partial}{\partial t}\bar{\rho}\tilde{e} + \nabla \cdot (\bar{\rho}\tilde{u}\tilde{e}) = -\bar{p}\nabla \cdot \tilde{u} + \bar{p}\nabla \cdot a - \nabla \cdot (\overline{\rho u''e''}) - \overline{p'\nabla \cdot u'} \quad (\text{A17})$$

$$\frac{\partial}{\partial t}\bar{\rho}\tilde{e} + \nabla \cdot (\bar{\rho}\tilde{u}\tilde{e}) = -\bar{p}\nabla \cdot \tilde{u} - a \cdot \nabla \bar{p} - \nabla \cdot (\overline{\rho u''h''}) + \overline{u' \cdot \nabla p'} \quad (\text{A18})$$

Now we see that the turbulent enthalpy flux is there depending on the formulation of turbulent work terms. In the BHR framework, neglecting the divergence of fluctuating velocity is permissible (and accurate in the limit of low turbulent mach number), and the implementation of the turbulent work has the same form as the bulk work. Thus we choose to diffuse only species internal energy and not species enthalpy in BHR-2.

-
- [1] J. Lindl, AIP Press. (1998).
 - [2] S. Gull, Mon. Not. R. Astr. Soc. **171**, 263 (1975).
 - [3] D. Besnard, F. H. Harlow, R. M. Rauenzahn, and C. Zemach, LANL Report **LA-12303-MS** (1992).
 - [4] H. von Helmholtz, Monatsberichte der Koniglichen Preussische Akademie der Wissenschaften zu Berlin **23**, 215 (1868).
 - [5] Rayleigh, Proceedings of the London Mathematical Society **14**, 170 (1883).
 - [6] R. Richtmyer, Communications on Pure and Applied Mathematics **13**, 297 (1960).
 - [7] K. Stalsberg-Zarling and R. A. Gore, LANL Report **LA-UR-11-04773** (2011).
 - [8] D. E. Burton, Lawrence Livermore National Laboratory Report **UCRL-JC-110555** (1992).
 - [9] D. E. Burton, Lawrence Livermore National Laboratory Report **UCRL-JC-118788** (1994).
 - [10] J. Waltz and T. Gianakon, Computer Physics Communications **183** (2012).
 - [11] E. Caramana, D. Burton, M. Shashkov, and P. Whalen, Journal of Computational Physics **146** (1998).
 - [12] J. Waltz, Numerical Methods for Multi-Material Fluids and Structures. Pavia, Italy (2009).
 - [13] A. Banerjee, R. A. Gore, and M. J. Andrews, Physical Review E **82** (2010).
 - [14] J. D. Schwarzkopf, D. Livescu, R. A. Gore, R. M. Rauenzahn, and J. R. Ristorcelli, Journal of Turbulence **12** (2011).
 - [15] G. Dimonte and R. Tipton, Physics of Fluids **18** (2006).
 - [16] A. W. Cook, Physics of Fluids **21** (2009).
 - [17] M. Gittings, R. Weaver, M. Clover, T. Betlach, N. Byrne, R. Coker, E. Dendy, R. Hueckstaedt, K. New, W. Oakes, et al., Comput. Sci. Disc. **1** (2008).
 - [18] B. Rollin and M. Andrews, In Preparation (2012).
 - [19] S. B. Pope, *Turbulent Flows* (Cambridge University Press, 2010).
 - [20] M. Andrews, Ph.D. Thesis, London University (1986).
 - [21] A. Banerjee, W. Kraft, and M. Andrews, J. Fluid Mech. **629**, 127 (2010).
 - [22] V. S. Smeeton and D. L. Youngs, AWE Report No. **O 35/87** (1987).
 - [23] M. Andrews and D. Spalding, Physics of Fluids A **2**, 922 (1986).
 - [24] V. C. N.V. Pitzyna, Yu.A. Kucherenko and A. Pylaev, Proceedings of the 4th International

- Workshop on the Physics of Compressible Turbulent Mixing (1993).
- [25] B. Rollin and M. Andrews, Proceedings of the ASME Fluids Engineering Summer Meeting (2012).
 - [26] T. Wei and D. Livescu, International Conference on Numerical Methods in Multiphase Flow, Penn State, PA. (2012).
 - [27] B. Rollin, N. Denissen, J. Reisner, and M. Andrews, Proceedings of the IMECE2012 (2012).